Enhanced CO_2 uptake at a shallow Arctic Ocean seep field overwhelms the positive warming potential of emitted methane

John W. Pohlman[a,1], Jens Greinert[b,c,d], Carolyn Ruppel[a], Anna Silyakova[c], Lisa Vielstädte[b], Michael Casso[a], Jürgen Mienert[c], and Stefan Bünz[c]

[a]U.S. Geological Survey, Woods Hole Coastal & Marine Science Center, Woods Hole, MA 02543; [b]Department of Marine Geosystems, GEOMAR Helmholtz Centre for Ocean Research, D-24148 Kiel, Germany; [c]Centre for Arctic Gas Hydrate, Environment and Climate, Department of Geosciences, University of Tromsø – The Arctic University of Norway, 9037 Tromso, Norway; and [d]Department of Marine Geology, Royal Netherlands Institute for Sea Research, AB Den Burg, Texel, Netherlands

Edited by Jonathan J. Cole, Cary Institute of Ecosystem Studies, Avon, NC, and approved March 8, 2017 (received for review November 15, 2016)

Continued warming of the Arctic Ocean in coming decades is projected to trigger the release of teragrams (1 Tg = 10^6 tons) of methane from thawing subsea permafrost on shallow continental shelves and dissociation of methane hydrate on upper continental slopes. On the shallow shelves (<100 m water depth), methane released from the seafloor may reach the atmosphere and potentially amplify global warming. On the other hand, biological uptake of carbon dioxide (CO_2) has the potential to offset the positive warming potential of emitted methane, a process that has not received detailed consideration for these settings. Continuous sea–air gas flux data collected over a shallow ebullitive methane seep field on the Svalbard margin reveal atmospheric CO_2 uptake rates (−33,300 ± 7,900 μmol $m^{-2}·d^{-1}$) twice that of surrounding waters and ∼1,900 times greater than the diffusive sea–air methane efflux (17.3 ± 4.8 μmol $m^{-2}·d^{-1}$). The negative radiative forcing expected from this CO_2 uptake is up to 231 times greater than the positive radiative forcing from the methane emissions. Surface water characteristics (e.g., high dissolved oxygen, high pH, and enrichment of ^{13}C in CO_2) indicate that upwelling of cold, nutrient-rich water from near the seafloor accompanies methane emissions and stimulates CO_2 consumption by photosynthesizing phytoplankton. These findings challenge the widely held perception that areas characterized by shallow-water methane seeps and/or strongly elevated sea–air methane flux always increase the global atmospheric greenhouse gas burden.

methane | carbon dioxide | greenhouse gas emissions | marine biogeochemistry | Arctic Ocean

Contemporary methane emissions from continental shelves to overlying oceans are estimated at 8 Tg to 65 Tg (1 Tg = 10^{12} g) annually (1), and will likely increase with future global warming. Inundation of high-latitude continental shelves accompanying sea level rise for the past ∼20 ka and superposed, shorter-lived warming events may be the triggers for ongoing methane release from thawing subsea permafrost, dissociating gas hydrate, and/or recent accumulations of microbial methane in newly warmed, organic-rich sediment (2–4). In deeper continental slope waters (200 m to 600 m) at high latitudes and midlatitudes, widespread methane seepage has been observed where warming intermediate ocean waters impinge on the shallowest extent of the gas hydrate stability zone (3, 5–9).

Methane emitted from seafloor seeps may exacerbate global warming if this potent greenhouse gas crosses the sea–air interface. However, most methane released at the seafloor may never reach the uppermost oceanic mixed layer due to a combination of gas exchange during the ascent of bubbles (10, 11), methane dissolution (12), and microbial oxidation of dissolved methane to carbon dioxide (13–15) (CO_2). The exception is methane emitted from the seabed in shallow-water marine settings (<100 m water depth), of which a substantial fraction may enter the atmosphere (2, 16, 17). Studies at these shallow-water locations have taken on urgency given their wide geographic distribution and potential for large emissions (18). On the other hand, little attention has been given to CO_2 exchange as a component of the net greenhouse gas flux balance at gas seepage sites. If CO_2 efflux is enhanced at seepage sites, it will have a positive effect on radiative forcing. On the other hand, if CO_2 is absorbed, it could mitigate the positive radiative effects from methane efflux.

In this study, we quantify methane and CO_2 sea–air fluxes along the western Svalbard margin (WSM) (Fig. 1*A*) to determine the net global warming potential for these two important greenhouse gases. The study was conducted in summer when light availability was unlimited, thereby maximizing the potential for CO_2 uptake by primary production (i.e., photosynthesis). The areas surveyed include a stable deep-water gas hydrate system (1,700 m to 2,600 m depth), a gas seepage area (240 m depth) suggested to be geologically linked to deeper climate-sensitive gas hydrate occurrences (5, 7, 19), a shallow-water (80 m to 90 m depth) active gas seep field along the ridge of a glacial moraine (19), and a nearshore (<110 m depth) coastal zone. These sites represent the full depth range of potential methane-emitting sites on high-latitude continental margins (3), including the potential for contributions from thawing subsea permafrost (4, 19).

Materials and Methods

In June 2014, we obtained a 1,600-km-long near-continuous record of methane and CO_2 concentrations and carbon isotopes from surface water of the WSM aboard the R/V *Helmer Hanssen* (Fig. 1*A*). These data, in addition to methane

Significance

Methane released from the seafloor and transported to the atmosphere has the potential to amplify global warming. At an arctic site characterized by high methane flux from the seafloor, we measured methane and carbon dioxide (CO_2) exchange across the sea–air interface. We found that CO_2 uptake in an area of elevated methane efflux was enhanced relative to surrounding waters, such that the negative radiative forcing effect (cooling) resulting from CO_2 uptake overwhelmed the positive radiative forcing effect (warming) supported by methane output. Our work suggests physical mechanisms (e.g., upwelling) that transport methane to the surface may also transport nutrient-enriched water that supports enhanced primary production and CO_2 drawdown. These areas of methane seepage may be net greenhouse gas sinks.

Author contributions: J.W.P., J.G., and S.B. designed research; J.W.P., J.G., A.S., and M.C. performed shipboard research; J.W.P., J.G., and M.C. contributed new reagents/analytic tools; J.W.P., J.G., C.R., and L.V. analyzed data; and J.W.P., J.G., C.R., and J.M. wrote the paper.

The authors declare no conflict of interest.

This article is a PNAS Direct Submission.

Data deposition: Archival data are available through the USGS ScienceBase-Catalog at https://doi.org/10.5066/F7M906V0.

[1]To whom correspondence should be addressed. Email: jpohlman@usgs.gov.

This article contains supporting information online at www.pnas.org/lookup/suppl/doi:10.1073/pnas.1618926114/-/DCSupplemental.

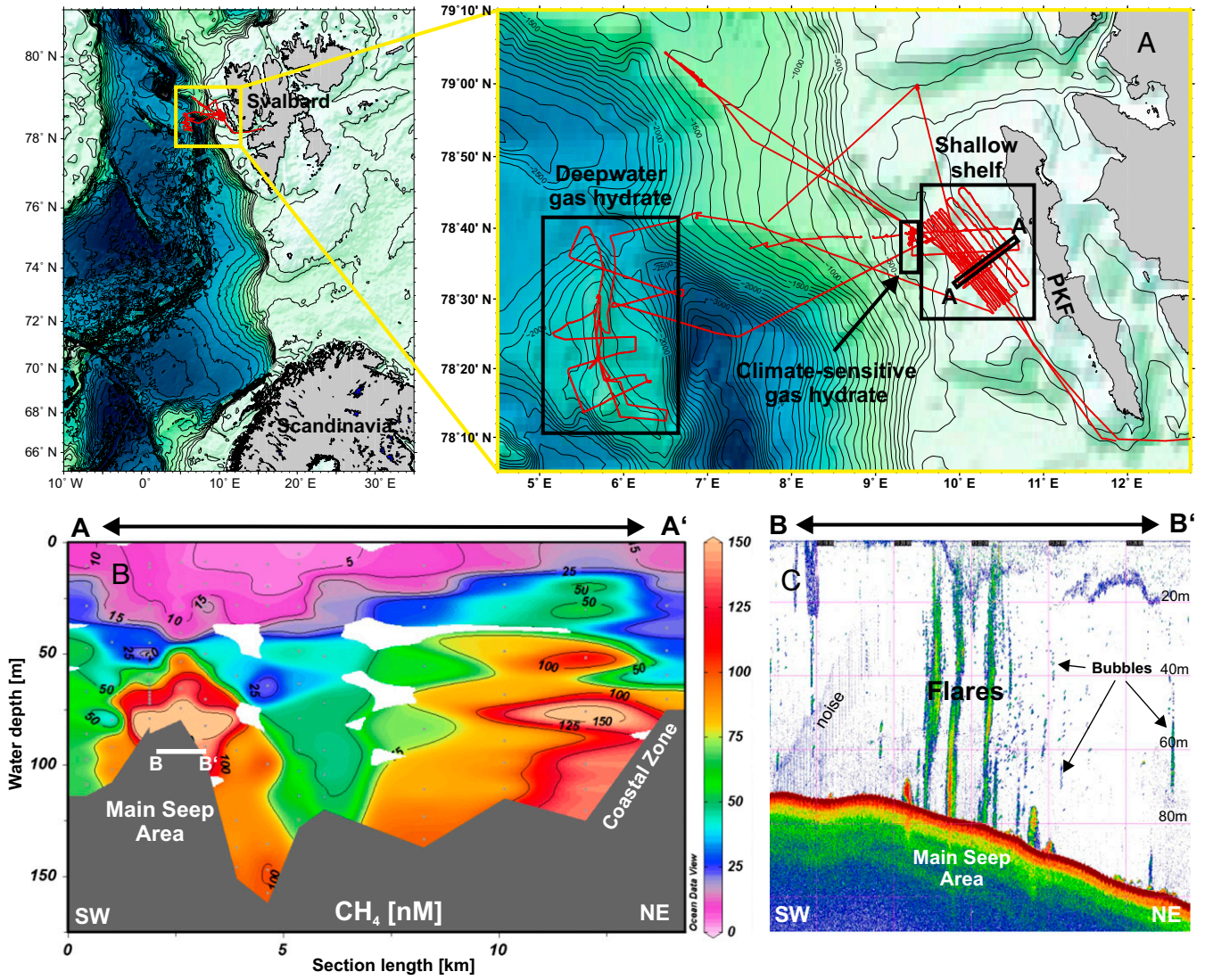

Fig. 1. Site map and water column methane offshore of western Svalbard during the CAGE 14-1 cruise. (*A*) Gas and gas hydrate sectors surveyed for methane flux, CO_2 flux, and water chemistry. Red lines are the survey tracklines. (*B*) Distribution of dissolved methane along transect A–A′ (see *A*). (*C*) Hydroacoustic evidence for gas flares and bubbles overlying the main seep area along transect B–B′ (see *B*). PKF, Prins Karls Forland.

and CO_2 concentrations from the atmospheric marine boundary layer, were acquired with the US Geological Survey-Gas Analysis System (USGS-GAS; *SI Appendix*, Fig. S1). The USGS-GAS is a dual cavity ring-down spectrometer (CRDS) analytical system that constantly circulates gas from the headspace of a Weiss-type equilibrator through a Picarro G-2201*i* CRDS and sequentially measures air concentrations received from intakes set at three to four different elevations on the ship exterior with a Picarro G-2301*f* CRDS. Stable carbon isotope values measured with the G-2201*i* were calibrated against standard gases to obtain accurate $\delta^{13}C$ values of surface water methane (±4‰ at 2 ppm; ±1.5‰ at 5 ppm) and CO_2 (±1.5‰). Gradients in methane and CO_2 concentrations were not detected in air samples collected at different elevations in the atmospheric marine boundary layer, so data from only one elevation (~22 m above the sea surface) are reported here. The gas concentration data were combined with meteorological (wind speed, air temperature) and sea surface water environmental parameters (salinity, water temperature; *SI Appendix*, Fig. S2) and averaged at 30-s intervals to determine the flux of methane and CO_2 across the sea–air interface (20) in shallow-water (Fig. 2) and deep-water (*SI Appendix*, Fig. S3) settings (21). To constrain biological activity in surface water, additional environmental parameters [dissolved oxygen (DO), pH, fluorescent dissolved organic matter (fDOM)] were measured in seawater pumped aboard the ship (*SI Appendix*, Table S4).

Surface water methane concentrations from 191 discrete water samples analyzed using the traditional gas chromatograph (GC) method and the USGS-GAS instrumentation were positively correlated ($r^2 = 0.86$, $P < 0.001$) with slope of 0.99 (Fig. 3), which indicates excellent agreement between the analytical methods. The SD of the difference between the methods was 2.1 nM, with a small, but significant, 0.48 nM ($P < 0.001$) bias toward lower values measured by the USGS-GAS system (*SI Appendix*, Fig. S7*A*). To provide constraints on the subsurface methane distribution and its environmental controls, we also acquired dissolved methane concentration (Fig. 1*B*) and conductivity-temperature-depth (CTD) vertical profiles (Fig. 4).

Greenhouse Gas Dynamics

Methane Concentration and Fluxes on the WSM. For the deep-water and shelf-edge systems (Fig. 1*A* and *SI Appendix*, Fig. S3), surface water methane concentrations ranged from 3.2 nM to 4.3 nM, corresponding to saturation anomalies of −1.5 to 36%. Sea–air fluxes ranged from 0.0 $\mu mol \cdot m^{-2} \cdot d^{-1}$ to 2.8 $\mu mol \cdot m^{-2} \cdot d^{-1}$ (Table 1 and *SI Appendix*, Fig. S3). The low saturation anomalies and fluxes for the 240-m water depth region are comparable to those in the open ocean (23) and are similar to those previously reported for this site (24), confirming that this setting is not a significant source of methane to the atmosphere.

The highest surface water methane concentrations (Fig. 2*A*) and dissolved-phase fluxes (Fig. 2*B*) were detected at the shallow

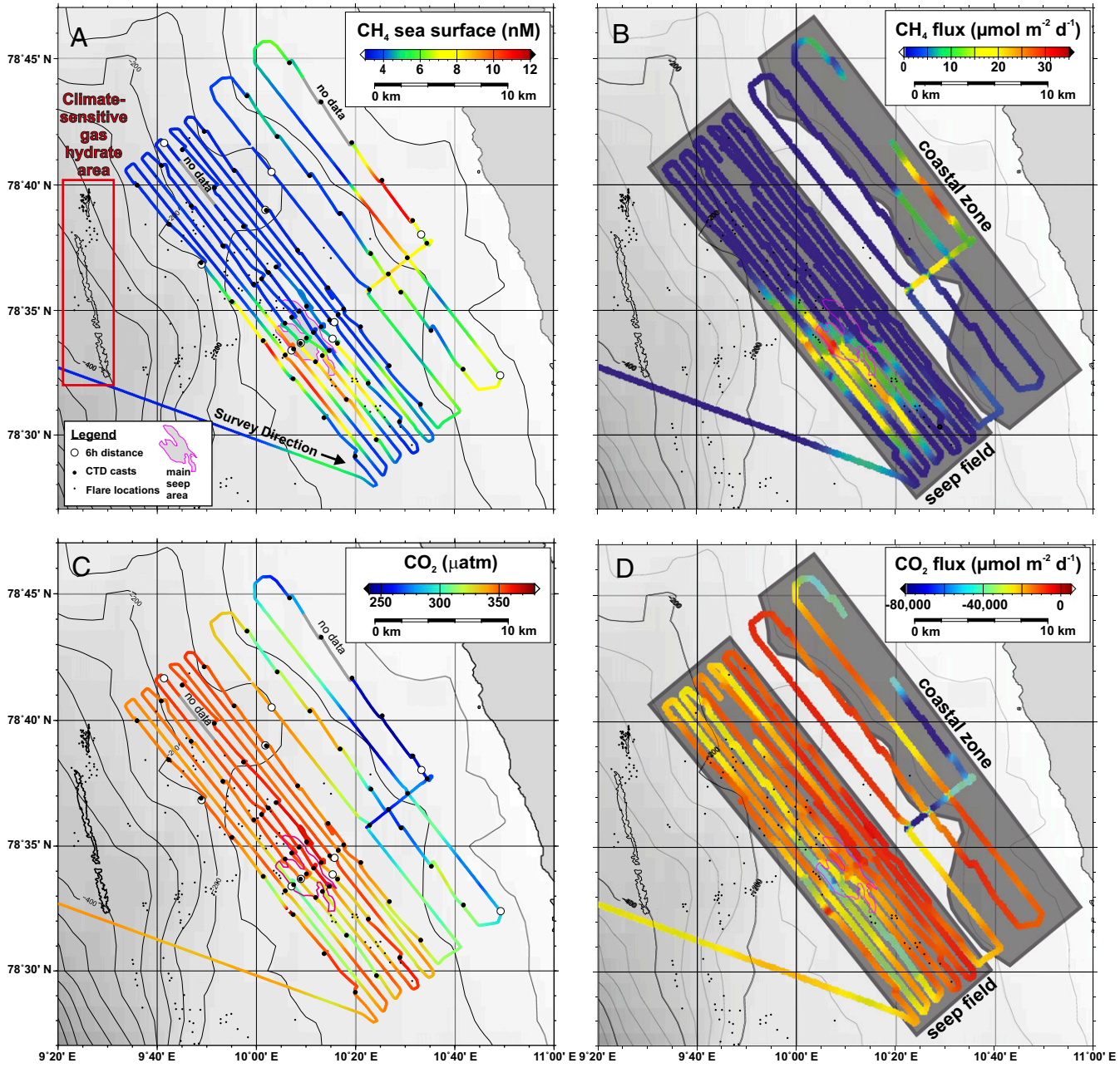

Fig. 2. Surface water methane and CO_2 concentration and flux at the shallow shelf site. (*A*) Methane concentration, (*B*) methane flux, (*C*) CO_2 concentration, and (*D*) CO_2 flux. Individual seep locations are indicated by small black dots. The main area of gas seepage containing multiple seeps is outlined with a solid pink line. Larger black dots located along the survey lines are the CTD hydrocast locations. White circles along the track line represent 6-h time intervals during the survey. The flux maps are partitioned into seep and coastal zones for the mass flux calculations in Table 1. The seaward limit of the coastal zone is bounded by the 110-m isobath. Within the seep zone, areas of high methane efflux and CO_2 influx (note negative values in the legend) are focused near the main seep area. *SI Appendix*, Fig. S3 contains flux maps for the climate-sensitive and deep-water gas hydrate areas.

continental shelf site ("Shallow shelf" in Fig. 1*A*), where gas bubbles emanate from a seep field on a glacial moraine at 80 m to 90 m water depth (Fig. 1*C*) and dissolved methane is released from the adjacent nearshore coastal zone seafloor (<110 m water depth). The median flux from more than 7,000 averaged intervals (30 s) for the shallow shelf was 3.9 $\mu mol \cdot m^{-2} \cdot d^{-1}$, which is similar to a median value of 3.5 $\mu mol \cdot m^{-2} \cdot d^{-1}$ calculated from hydrocast samples collected from 10 m water depth (25). In the seep field, methane concentrations ranged from 3.4 nM to 10.8 nM (Fig. 2*A*), representing an 8 to 235% saturation anomaly and supporting a sea–air flux of 0.1 $\mu mol \cdot m^{-2} \cdot d^{-1}$ to 31.8 $\mu mol \cdot m^{-2} \cdot d^{-1}$ (Fig. 2*B* and Table 1). Where the diffusive sea–air methane flux exceeded 10 $\mu mol \cdot m^{-2} \cdot d^{-1}$ in the seep field ("high-flux" region in Table 1), values average 17.3 ± 4.8 $\mu mol \cdot m^{-2} \cdot d^{-1}$, almost 9 times greater than the background flux of 2.0 ± 1.9 $\mu mol \cdot m^{-2} \cdot d^{-1}$ (Table 1). Methane concentrations in the nearshore coastal zone ranged from 3.2 nM to 11.0 nM (Fig. 2*A*), with corresponding sea–air fluxes of 0.1 $\mu mol \cdot m^{-2} \cdot d^{-1}$ to 28.7 $\mu mol \cdot m^{-2} \cdot d^{-1}$ (Fig. 2*B* and Table 1).

Gridded and normalized to an area of 100 km^2, the daily sea–air methane flux from each area ranged from 0.5 kg to 8.8 kg per 100 km^2, with highest values in the nearshore (*SI Appendix*, Table S1). In the context of a well-constrained global atmospheric methane source (e.g., ruminants), the flux from the shallow-water

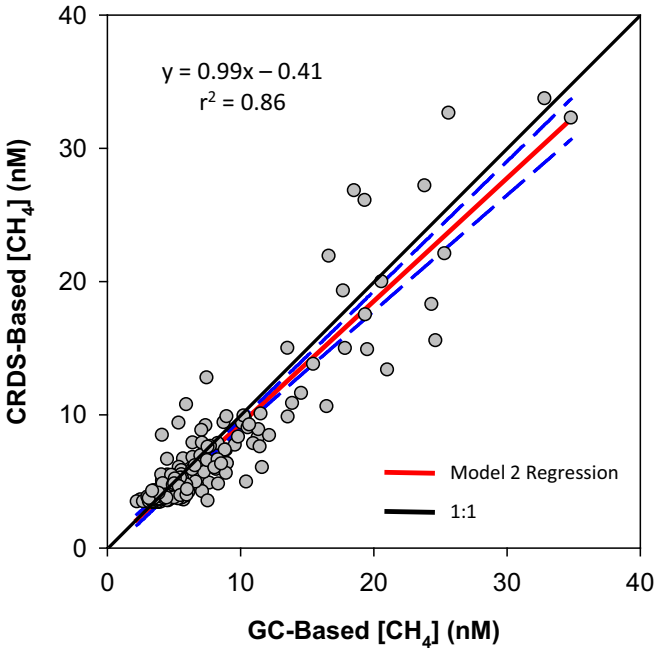

Fig. 3. Regression analysis for GC-based and CRDS-based measurements; 191 methane concentration measurements of discrete samples determined by the GC headspace analysis method compared with values obtained from the continuously measuring USGS-GAS. Blue dashed lines are the 95% confidence interval for the model 2 regression. There was a slight negative bias (−0.5 nM, $P < 0.001$) for the CRDS-based measurement, as determined by the Bland Altman agreement analysis (22) (*SI Appendix*, Fig. S7).

continental shelf seep field [6.1 kg CH_4 (100 km^{-2})·d^{-1}, *SI Appendix*, Table S1] is equivalent to that from ~320 sheep, each emitting 18.9 g CH_4 d^{-1} (26). To match the methane output of the 3×10^7 sheep in New Zealand alone would require more than 90,000 multiseep clusters of the type investigated here. Although tens of thousands of discrete seeps likely remain undiscovered on global margins (8), there is no evidence that such a large number of multiseep clusters exists. Even if there were, the annual cumulative atmospheric methane flux would be ~0.15 Tg CH_4 y^{-1}, a negligible (0.03%) quantity relative to the 580 Tg of methane emitted to the atmosphere annually (18).

WSM Fluxes Compared with Siberian Shelf Seas. Our data show that shallow arctic methane seeps like those we investigated on the WSM emit negligible methane to the atmosphere. However, in comparison with the seeps we investigated, methane fluxes from the shallow East Siberian Arctic Shelf (ESAS), which may be underlain by thawing subsea permafrost, are ~100 times greater. Shakhova et al. (2) report average fluxes of 229 μmol·m^{-2}·d^{-1} for "background" areas and 738 μmol·m^{-2}·d^{-1} from "hotspots" during the ice-free summertime. These values are comparable to an average ice-free flux for the middle and outer East Siberian Arctic shelf of 238 μmol·m^{-2}·d^{-1}, as measured by Thornton et al. (17). Given that (*i*) gas flares (evidence of seafloor gas ebullition) are prominent features on the WSM (ref. 15 and Fig. 1*C*) and ESAS (2), (*ii*) maximum bottom-water methane concentrations at the WSM seeps (Fig. 1*B*; ~300 nM) are comparable to summertime bottom-water concentrations in ESAS hotspots (2), and (*iii*) WSM gas could also have a component derived from thawing subsea permafrost (4, 19), it is difficult to reconcile why the diffusive fluxes we report from the WSM differ so greatly from those of the ESAS. Methane may be more rapidly oxidized from the WSM water column (13, 24); however, a more likely explanation is that lateral transport of methane from the relatively small and narrow WSM shelf dilutes and disperses methane into the deeper ocean. Similar dispersion and dilution on the shallow, expansive ESAS is not possible, which could permit a greater fraction of methane released from the seafloor to transfer to the atmosphere.

CO_2 Flux and Net Global Warming Potential Flux on the WSM. Within the shallow-water gas seep field, pCO_2 in the surface water was substantially less than in the surrounding area (Figs. 2 *C* and *D* and 5*A*) and correlates negatively with methane concentration (r^2 = 0.61; *SI Appendix*, Fig. S4). These undersaturated pCO_2 values support a CO_2 influx rate of −33,300 ± 7,900 μmol·m^{-2}·d^{-1} (Table 1), which is about twice that of the surrounding background area (−16,000 ± 6,000 μmol·m^{-2}·d^{-1}) and more than 1,900 times greater than the efflux of methane (17.3 ± 4.8 μmol·m^{-2}·d^{-1}). Taking into account the 25 times greater global warming potential

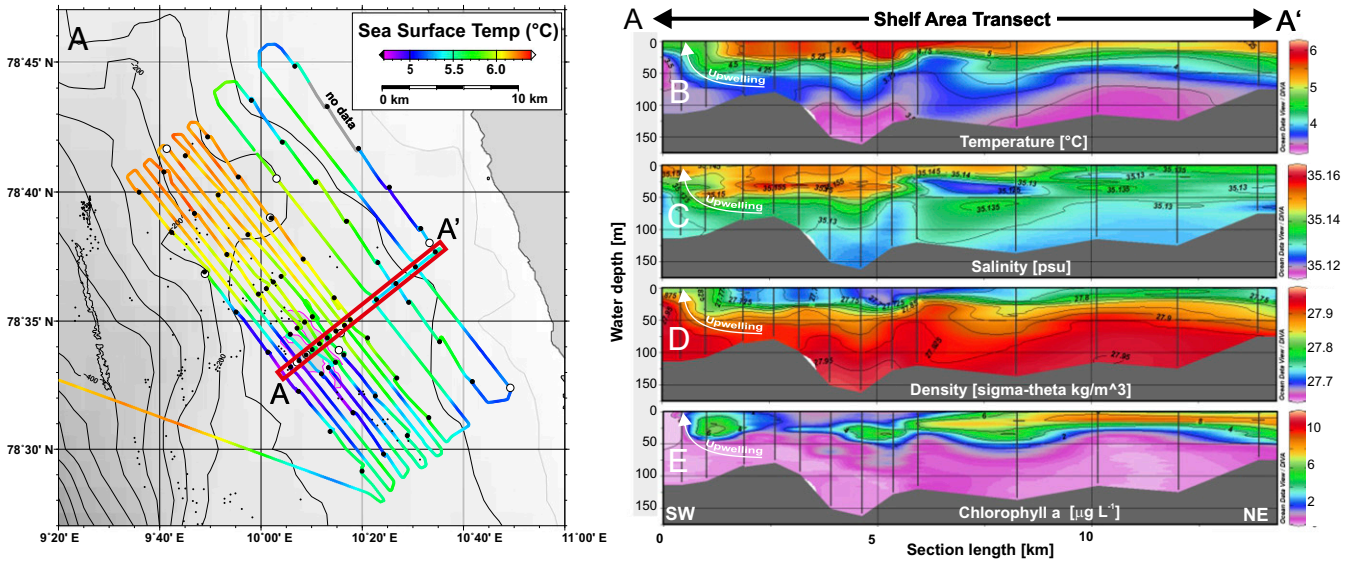

Fig. 4. Physicochemical water properties of the shallow shelf area. (*A*) Sea surface temperature (SST) during the shallow shelf survey. Colder surface water corresponds with the high-methane, low-CO_2 surface water in Fig. 2. Shore-perpendicular distributions of (*B*) temperature, (*C*) salinity, (*D*) density, and (*E*) chlorophyll concentration along transect A–A′ show that colder bottom water upwells along steeply tilted isopycnals near the termination of a warm surface-water lens extending from the coastline. Elevated chlorophyll fluorescence was observed within the upwelling region.

Table 1. Methane and CO_2 fluxes for areas investigated in this study

Setting	Survey area (km^2)	CH_4 flux ($\mu mol \cdot m^{-2} \cdot d^{-1}$)	CO_2 flux ($\mu mol \cdot m^{-2} \cdot d^{-1}$)
Shallow shelf seep field			
All	150.5	3.8 ± 5.5	−18,037 ± 8,464
High flux*	17.6	17.3 ± 4.8	−33,317 ± 7,927
Background	132.9	2.0 ± 1.9	−16,017 ± 6,152
Nearshore coastal zone	38.7	5.5 ± 6.5	−24,944 ± 17,818
Deep shelf seeps	11.5	0.30 ± 0.26	−2,166 ± 1,117
Deep-water gas hydrate	112	1.05 ± 0.61	−42,001 ± 24,528

See *SI Appendix*, Table S1 for additional site summary details.
*High flux defined as areas with CH_4 flux > 10 $\mu mol \cdot m^{-2} \cdot d^{-1}$.

of methane relative to CO_2 for a 100-y timescale on a per unit mass basis (18), the strongly negative CO_2 flux at the seep offsets the positive effect of methane expelled by a factor of 231 despite methane's greater global warming potential. Even on a 25-y timescale, for which methane has stronger GWP of 84 (18), the cooling effect of CO_2 uptake is 69 times greater than methane's warming effect. Our comparisons consider only the dissolved phase gas fluxes. However, hydroacoustic imaging (Fig. 1*C*) and bubble modeling (*SI Appendix*, Fig. S8*A*) suggest minimal direct bubble transport to the atmosphere. Furthermore, a recent study from the ESAS suggesting that turbulence-driven diffusive methane flux (not ebullition) is the primary transport mechanism for sea–air methane flux (17) supports our assessment that bubble transport of methane to the atmosphere is not important at this setting.

Stimulation of CO_2 Uptake over Shallow-Water Methane Seeps. At least two processes could be responsible for the reduced concentrations of CO_2 observed over the shallow-water methane seeps: (*i*) Methane bubbles ascending from the seafloor dissolve methane, strip CO_2 from the water column, and transport this CO_2 to the sea–air interface and release it to the atmosphere (12), or (*ii*) a physical and/or biological mechanism stimulates photosynthesis, and thus CO_2 drawdown, above the seep area. To test the first hypothesis, we applied a numerical bubble-stripping model (12). Reproducing the low CO_2 concentrations requires (*i*) bubble diameters of 14 mm, which is much larger than the most frequent diameter of ∼6 mm (range 2 mm to 16 mm) observed in the area (27), and (*ii*) a volumetric gas flux of 34 $L \cdot m^{-2} \cdot min^{-1}$ from the seabed at 90 m (∼13.6 mol/min, at 4 °C), compared with reported values of 3 $mL \cdot min^{-1}$ to 41 $mL \cdot min^{-1}$ per seep at 385 m (5.4 mmol/min to 74.5 mmol/min, at 4 °C) (19). Bubble stripping is therefore not a plausible mechanism for removing CO_2.

The alternate hypothesis for lower surface-water pCO_2 is that upwelling of cold, nutrient-rich water stimulated CO_2 assimilation by phytoplankton, a phenomenon also observed in areas of strong upwelling associated with eastern boundary currents of major ocean basins (28). Surface water within the high-methane, low-CO_2 seep area was 0.65 °C colder than the surrounding surface water (Figs. 4*A* and 5*C* and *SI Appendix*, Table S1), and the estimated $\delta^{13}C$ of the seabed-sourced methane measured at the sea surface (−54.6‰; *SI Appendix*, *Methane Isotopic Mass Balance for Determination of Seabed*) was similar to that reported at the seafloor (29) and emanating from seeps downslope (19). We are therefore confident the cold and methane-rich surface water originated from near the seafloor close to the seep area. Furthermore, CO_2 uptake rates we measured (2,200 $\mu mol \cdot m^{-2} \cdot d^{-1}$ to 42,000 $\mu mol \cdot m^{-2} \cdot d^{-1}$; Table 1) are comparable to primary production rates reported from nearby Kongsfjorden (30) (600 $\mu mol \cdot m^{-2} \cdot d^{-1}$ to 184,000 $\mu mol \cdot m^{-2} \cdot d^{-1}$), confirming the plausibility that phytoplankton-related processes altered the surface water CO_2 budget. A possible subsurface manifestation of high surface productivity is that benthic chlorophyll and phaeopigment concentrations at this seep were the highest among nine stations investigated in the western Svalbard–Barents Sea region (31).

Upwelling on the WSM shelf is driven by Ekman transport during northerly or onshore wind events that can occur during any season (32). On a smaller scale, the topographically steered Spitsbergen Polar Current encountering the high-relief glacial moraine may upwell locally along steeply tilted isopycnals (Fig. 4*D*). Bubble-driven buoyancy and entrainment of bottom waters may also transport bottom water to the photic zone from depths as great as 1,000 m (33), a mechanism invoked to explain elevated surface-water chlorophyll above a Gulf of Mexico hydrocarbon seep (34). The relatively low seafloor methane flux at the WSM seep sites between 240 m and 385 m water depth (19) renders it unlikely that bubble-associated buoyancy caused the upwelling, supporting the assumption that physical oceanographic processes alone are responsible for upwelling, independent of the presence of gas seepage.

Regardless of the upwelling mechanism, multiple lines of evidence support the interpretation that primary production and consequent CO_2 drawdown are enhanced where methane-charged bottom water emerges: (*i*) Chlorophyll-fluorescence, a proxy for photosynthesis, is elevated (Fig. 4*E*); (*ii*) DO, a product of photosynthesis, is ∼1 mg/L higher in surface waters with high methane and low CO_2 concentrations (Fig. 5*D*); (*iii*) pH, which increases when CO_2 is removed from solution by photosynthesis, is elevated by as much as 0.6 units compared with background (Fig. 5*D*); and (*iv*) $\delta^{13}C$–CO_2, a metric that becomes more

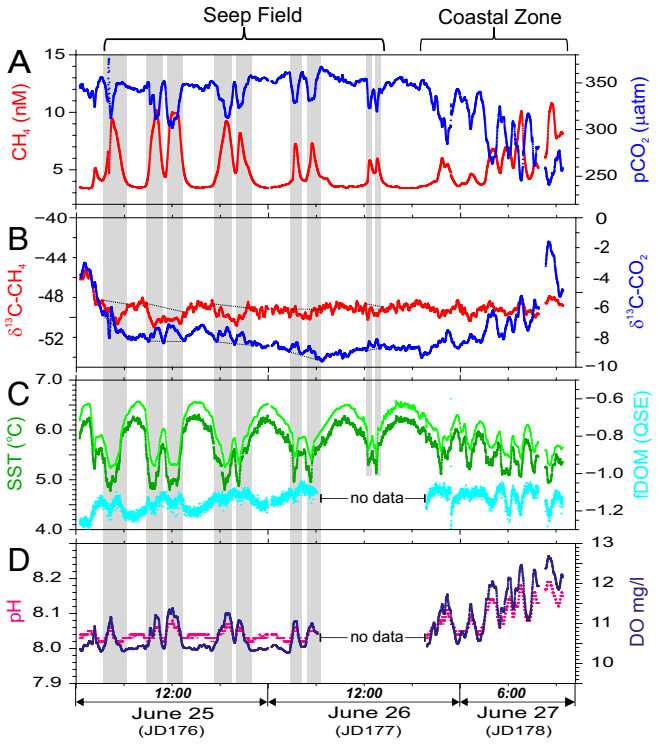

Fig. 5. Surface water time series data for the shallow shelf survey. (*A*) Dissolved methane concentration and pCO_2; (*B*) $\delta^{13}C$–CH_4 and $\delta^{13}C$–CO_2; (*C*) SST temperature [dark green, hull-mounted sensor; light green, EXO2 sensor (YSI Incorported)] and fDOM; and (*D*) pH and DO. Seep crossings (highlighted with gray bars) are characterized by colder water containing elevated concentrations of ^{13}C-depleted methane and lower concentrations of ^{13}C-enriched CO_2. Isotopic excursions are demarcated by dashed lines that connect $\delta^{13}C$ values from the margins of the seep crossings. Within the seep crossings, fDOM, pH, and DO are elevated. The combined evidence suggests upwelling of cold, methane-charged (and presumably nutrient-rich) bottom water originating from the seep-stimulated phytoplankton activity in the surface water that enhanced the consumption of CO_2. Similar trends occur within the nearshore coastal zone.

positive when algae preferentially remove $^{12}CO_2$ during photosynthesis, is ^{13}C-enriched (more positive) by as much as 2‰ within the upwelling area of methane-charged bottom water (Fig. 5*B*).

Similar, yet more pronounced, patterns of high methane, low CO_2, and changes in water chemistry indicative of upwelling-induced photosynthesis were observed in the nearshore coastal zone (Fig. 5 and *SI Appendix*, Fig. S4). However, the coastal zone lacks pervasive discrete bubble-releasing methane seeps (Fig. 2*A*). Most methane in that region (up to 150 nM in bottom waters; Fig. 1*B*) likely originates from in situ production in organic-rich, anoxic sediment. Elevated methane in marine surface waters can also be a product of dimethylsulfoniopropionate demethylation (35), but the high bottom-water methane content and $\delta^{13}C$ signature of the nearshore methane are most consistent with a sediment source.

Despite the spatiotemporal coincidence between high concentrations of methane and enhanced CO_2 uptake at seeps on the WSM continental shelf (Fig. 5*A*) and in some other settings such as the Santa Barbara Basin seep field (36), we suggest that high methane concentrations are an indicator of, but not a necessary condition for, enhanced CO_2 drawdown. Instead, the surface-water methane observed on the WSM is a chemical tracer for cold, nutrient-rich upwelled water that supports enhanced photosynthesis within the euphotic zone. A relationship of higher methane efflux and CO_2 influx that correlated with colder surface waters was also observed near the >2,000-m deep-water gas hydrate site (*SI Appendix*, Fig. S5). This observation suggests enhanced CO_2 drawdown is likely to occur whenever deep nutrient-rich (and perhaps methane-charged) waters are upwelled to the surface, and conditions for photosynthesis are suitable.

Methane seepage from high-latitude shallow continental margins is an atmospheric methane source (2) that could become more substantial as the climate continues to warm. Evidence that the cooling potential from CO_2 influx at this shallow-water arctic methane seep overwhelms the greenhouse warming potential from the emitted methane suggests that methane seeps can nevertheless be net sinks for climate-forcing gases. If the sedimentary efflux of nutrients that support photosynthesis is related to methane discharge intensity from the seafloor, a positive feedback between accelerated methane release from the seafloor and amplified atmospheric warming may be offset by atmospheric CO_2 drawdown. Further investigation of sea–air greenhouse gas fluxes at methane seep sites where upwelling-driven outputs are counteracted by photosynthetic CO_2 drawdown (including light-limited wintertime conditions) would provide data to constrain which processes are responsible for enhanced CO_2 uptake, quantify net greenhouse gas fluxes globally for shallow-water methane seepage areas, and determine if accelerated seafloor methane release will be offset by enhanced CO_2 uptake at the sea–air interface in the future.

ACKNOWLEDGMENTS. E. Bergeron, E. Moore, and P. Bernard at the USGS contributed engineering and logistical expertise that led to the successful completion of this project. We thank Andrea Bodenbinder and Mario Veloso from GEOMAR for providing technical assistance. J.W.P., C.R., and M.C. were supported by the USGS and interagency agreements DE-FE0002911 and DE-FE0005806 with the US Department of Energy. A.S., J.M., and S.B., as well as R/V *Helmer Hanssen* cruise costs, were supported by University of Tromsø – The Arctic University of Norway and the Research Council of Norway. The research is part of the Centre for Arctic Gas Hydrate, Environment and Climate and was supported by the Research Council of Norway through its Centres of Excellence funding scheme Grant 223259. Any use of trade names is for descriptive purposes and does not imply endorsement by the US government.

1. Hovland M, Judd AG, Burke RA (1993) The global flux of methane from shallow submarine sediments. *Chemosphere* 26:559–578.
2. Shakhova N, et al. (2010) Extensive methane venting to the atmosphere from sediments of the East Siberian Arctic Shelf. *Science* 327:1246–1250.
3. Ruppel CD, Kessler JD (2017) The interaction of climate change and methane hydrates. *Rev Geophys* 55(1):126–168.
4. Portnov A, Vadakkepuliyambatta S, Mienert J, Hubbard A (2016) Ice-sheet-driven methane storage and release in the Arctic. *Nat Commun* 7:10314.
5. Westbrook GK, et al. (2009) Escape of methane gas from the seabed along the West Spitsbergen continental margin. *Geophys Res Lett* 36:L15608.
6. Ferré B, Mienert J, Feseker T (2012) Ocean temperature variability for the past 60 years on the Norwegian-Svalbard margin influences gas hydrate stability on human time scales. *J Geophys Res-Oceans* 117:C10017.
7. Berndt C, et al. (2014) Temporal constraints on hydrate-controlled methane seepage off Svalbard. *Science* 343:284–287.
8. Skarke A, Ruppel C, Kodis M, Brothers D, Lobecker E (2014) Widespread methane leakage from the sea floor on the northern US Atlantic margin. *Nat Geosci* 7:657–661.
9. Phrampus BJ, Hornbach MJ, Ruppel CD, Hart PE (2014) Widespread gas hydrate instability on the upper U.S. Beaufort margin. *J Geophys Res Solid Earth* 119: 8594–8609.
10. McGinnis DF, Greinert J, Artemov Y, Beaubien SE, Wuest A (2006) Fate of rising methane bubbles in stratified waters: How much methane reaches the atmosphere? *J Geophys Res-Oceans* 111:C09007.
11. Rehder G, Leifer I, Brewer PG, Friederich G, Peltzer ET (2009) Controls on methane bubble dissolution inside and outside the hydrate stability field from open ocean field experiments and numerical modeling. *Mar Chem* 114:19–30.
12. Vielstadte L, et al. (2015) Quantification of methane emissions at abandoned gas wells in the Central North Sea. *Mar Pet Geol* 68:848–860.
13. Steinle L, et al. (2015) Water column methanotrophy controlled by a rapid oceanographic switch. *Nat Geosci* 8:378–382.
14. Kessler JD, et al. (2011) A persistent oxygen anomaly reveals the fate of spilled methane in the deep Gulf of Mexico. *Science* 331:312–315.
15. Ward BB, Kilpatrick KA, Novelli PC, Scranton MI (1987) Methane oxidation and methane fluxes in the ocean surface layer and deep anoxic waters. *Nature* 327:226–229.
16. Shakhova N, et al. (2014) Ebullition and storm-induced methane release from the East Siberian Arctic Shelf. *Nat Geosci* 7:64–70.
17. Thornton BF, Geibel MC, Crill PM, Humborg C, Morth CM (2016) Methane fluxes from the sea to the atmosphere across the Siberian shelf seas. *Geophys Res Lett* 43: 5869–5877.
18. Intergovernmental Panel on Climate Change (2013) *Climate Change 2013: The Physical Science Basis. Contribution of Working Group I to the Fifth Assessment Report of the Intergovernmental Panel on Climate Change* (Cambridge Univ Press, Cambridge, UK).
19. Sahling H, et al. (2014) Gas emissions at the continental margin west of Svalbard: Mapping, sampling, and quantification. *Biogeosciences* 11:6029–6046.
20. Wanninkhof R (1992) Relationship between wind speed and gas exchange over the ocean. *J Geophys Res-Oceans* 97:7373–7382.
21. Wanninkhof R, Asher WE, Ho DT, Sweeney C, McGillis WR (2009) Advances in quantifying air-sea gas exchange and environmental forcing. *Annu Rev Mar Sci* 1: 213–244.
22. Bland JM, Altman DG (1986) Statistical methods for assessing agreement between two methods of clinical measurement. *Lancet* 1:307–310.
23. Tilbrook BD, Karl DM (1995) Methane sources, distributions and sinks from California coastal waters to the oligotrophic North Pacific gyre. *Mar Chem* 49:51–64.
24. Graves CA, et al. (2015) Fluxes and fate of dissolved methane released at the seafloor at the landward limit of the gas hydrate stability zone offshore western Svalbard. *J Geophys Res-Oceans* 120:6185–6201.
25. Myhre CL, et al. (2016) Extensive release of methane from Arctic seabed west of Svalbard during summer 2014 does not influence the atmosphere. *Geophys Res Lett* 43:4624–4631.
26. Lassey KR, Ulyatt MJ, Martin RJ, Walker CF, Shelton ID (1997) Methane emissions measured directly from grazing livestock in New Zealand. *Atmos Environ* 31: 2905–2914.
27. Veloso M, Greinert J, Mienert J, De Batist M (2015) A new methodology for quantifying bubble flow rates in deep water using splitbeam echosounders: Examples from the Arctic offshore NW-Svalbard. *Limnol Oceanogr Methods* 13:267–287.
28. Capone DG, Hutchins DA (2013) Microbial biogeochemistry of coastal upwelling regimes in a changing ocean. *Nat Geosci* 6:711–717.
29. Damm E, Schauer U, Rudels B, Haas C (2007) Excess of bottom-released methane in an Arctic shelf sea polynya in winter. *Cont Shelf Res* 27:1692–1701.
30. Piwosz K, Pernthaler J (2010) Seasonal population dynamics and trophic role of planktonic nanoflagellates in coastal surface waters of the Southern Baltic Sea. *Environ Microbiol* 12:364–377.
31. Astrom EKL, Carroll ML, Ambrose WG, Carroll J (2016) Arctic cold seeps in marine methane hydrate environments: impacts on shelf macrobenthic community structure offshore Svalbard. *Mar Ecol Prog Ser* 552:1–18.
32. Nilsen F, Skogseth R, Vaardal-Lunde J, Inall M (2016) A simple shelf circulation model: Intrusion of Atlantic water on the West Spitsbergen shelf. *J Phys Oceanogr* 46:1209–1230.
33. Leifer I, Jeuthe H, Gjøsund SH, Johansen V (2009) Engineered and natural marine seep, bubble-driven buoyancy flows. *J Phys Oceanogr* 39:3071–3090.
34. D'Souza NA, et al. (2016) Elevated surface chlorophyll associated with natural oil seeps in the Gulf of Mexico. *Nat Geosci* 9:215–218.
35. Damm E, Kiene RP, Schwarz J, Falck E, Dieckmann G (2008) Methane cycling in Arctic shelf water and its relationship with phytoplankton biomass and DMSP. *Mar Chem* 109:45–59.
36. Du M, et al. (2014) High resolution measurements of methane and carbon dioxide in surface waters over a natural seep reveal dynamics of dissolved phase air-sea flux. *Environ Sci Technol* 48:10165–10173.